A comprehensive survey of 3′ animal miRNA modification events and a possible role for 3 ′ adenylation in modulating miRNA targeting effectiveness

A. Maxwell Burroughs, Yoshinari Ando, Michiel J.L. de Hoon, et al.

Genome Res. 2010 20: 1398-1410 originally published online August 18, 2010
Access the most recent version at doi:10.1101/gr.106054.110

A comprehensive survey of 3′ animal miRNA modification events and a possible role for 3′ adenylation in modulating miRNA targeting effectiveness

A. Maxwell Burroughs,[1,4,5] Yoshinari Ando,[1,4,5] Michiel J.L. de Hoon,[1] Yasuhiro Tomaru,[1,2] Takahiro Nishibu,[3] Ryo Ukekawa,[3] Taku Funakoshi,[3] Tsutomu Kurokawa,[3] Harukazu Suzuki,[1] Yoshihide Hayashizaki,[1,2] and Carsten O. Daub[1]

[1]*Omics Science Center (OSC), RIKEN Yokohama Institute, Tsurumi-ku, Yokohama-shi, Kanagawa 230-0045, Japan;* [2]*International Graduate School of Arts and Science, Yokohama City University, Tsurumi-ku, Yokohama-shi, Kanagawa 230-0045, Japan;* [3]*Wako Pure Chemical Industries, Ltd., Chuo-ku, Osaka 540-8605, Japan*

Animal microRNA sequences are subject to 3′ nucleotide addition. Through detailed analysis of deep-sequenced short RNA data sets, we show adenylation and uridylation of miRNA is globally present and conserved across *Drosophila* and vertebrates. To better understand 3′ adenylation function, we deep-sequenced RNA after knockdown of nucleotidyltransferase enzymes. The PAPD4 nucleotidyltransferase adenylates a wide range of miRNA loci, but adenylation does not appear to affect miRNA stability on a genome-wide scale. Adenine addition appears to reduce effectiveness of miRNA targeting of mRNA transcripts while deep-sequencing of RNA bound to immunoprecipitated Argonaute (AGO) subfamily proteins EIF2CI–EIF2C3 revealed substantial reduction of adenine addition in miRNA associated with EIF2C2 and EIF2C3. Our findings show 3′ addition events are widespread and conserved across animals, PAPD4 is a primary miRNA adenylating enzyme, and suggest a role for 3′ adenine addition in modulating miRNA effectiveness, possibly through interfering with incorporation into the RNA-induced silencing complex (RISC), a regulatory role that would complement the role of miRNA uridylation in blocking DICER1 uptake.

[Supplemental material is available online at http://www.genome.org. The sequencing data from this study have been submitted to the DDBJ Sequence Read Archive (DRA) (http://trace.ddbj.nig.ac.jp/dra/index_e.shtml) under accession no. DRA000205.]

The genomes of most animal species encode for mature microRNA (miRNA) (Grimson et al. 2008), a distinct class of 20–24-nucleotide (nt) base pair single-stranded noncoding RNA (ncRNA) which post-transcriptionally regulates messenger RNA (mRNA) copy level and translation efficiency through complementary binding of small stretches of base pairs typically in the 3′ untranslated region (UTR). In plants, several studies have implicated 3′ modification of mature miRNA as important to the stability of the miRNA (Li et al. 2005; Ramachandran and Chen 2008; Lu et al. 2009). miRNA deep sequencing experiments based on second-generation sequencing technologies suggested that a fraction of animal miRNAs may be subject to 3′ modification through addition of small numbers of nucleotides (Landgraf et al. 2007). While 3′ modifications in the form of adenine and uridine addition were observed, their biological role and the extent to which these modifications occur on a genome-wide scale remain poorly understood.

Recently, the PAPD4 (also referred to as GLD-2) ribonucleotidyltransferase enzyme was shown to add a single adenine residue to liver-specific expressed miR-122 in humans and mice (Katoh et al. 2009). PAPD4 is a so-called "noncanonical" transferase (Martin and Keller 2007) belonging to the TRF family of nucleotidyltransferases (Aravind and Koonin 1999). Individual members of this unusual family of enzymes have displayed remarkable substrate flexibility, having often been implicated in modification of substrates belonging to distinct classes of coding and/or noncoding RNA moieties in the cell (Martin and Keller 2007). In at least one instance, the same enzyme has demonstrated the capacity to catalyze the addition of both uridine and adenine to different substrates (Trippe et al. 1998; Mellman et al. 2008).

To better define the global contours of 3′ miRNA addition, we prepared short RNA libraries of human THP-1 monocytic cells and compared these with other publicly available deep-sequenced short RNA libraries. We also constructed libraries that were subject to siRNA-mediated knockdown of different nucleotidyltransferases, including PAPD4. To examine the biological role for adenine addition to the 3′ end of miRNA, we examined their association with Argonaute proteins, a crucial interaction required for miRNAs to perform their regulatory role.

Results

Probing the evolutionary depth of 3′ animal miRNA addition

We deep-sequenced a short RNA library from THP-1 monocytic cells using an Illumina GAII sequencer and mapped the extracted tags to individual miRNA loci. We also subjected raw data from

[4]**These authors contributed equally to this work.**
[5]**Corresponding authors.**
E-mail burrough@gsc.riken.jp; fax 81-(0)-45-503-9216.
E-mail yando@gsc.riken.jp; fax 81-(0)-45-503-9216.
Article published online before print. Article and publication date are at http://www.genome.org/cgi/doi/10.1101/gr.106054.110. Freely available online through the *Genome Research* Open Access option.

20:1398–1410 © 2010 by Cold Spring Harbor Laboratory Press; ISSN 1088-9051/10; www.genome.org

publicly available short RNA libraries derived from human HeLa, MCF-7, and U2OS cells (Mayr and Bartel 2009), mouse embryonic stem cells (ES) (Marson et al. 2008), chicken embryo cells (Glazov et al. 2008), and *Drosophila* head tissue (Ghildiyal et al. 2010) to the same mapping procedure. To avoid cross-mapping of tags between closely related miRNA loci, for each data set we applied a cross-mapping correction algorithm (De Hoon et al. 2010) while allowing for up to two mismatches.

Three prime nucleotide additions identified from deep-sequenced RNA libraries may be "ambiguous" or "unambiguous" depending on the DNA sequence at the cognate position in the genome. Ambiguous addition occurs when nucleotides observed at the 3′ end of the mature sequence align to cognate positions in the genome. Ambiguous addition could conceivably result from differential cutting via ribonuclease domains during the miRNA maturation process, post-maturation modification via nucleotidyltransferase-mediated nucleotide addition, or some combination of these two processes. Unambiguous addition occurs when extra nucleotides located at the 3′ miRNA end do not have a cognate nucleobase at the corresponding position in the genome; these are most likely added through nucleotidyltransferase action following maturation. Instances of all possible combinations of both ambiguous and unambiguous single and double nucleotide 3′ addition were tallied at each miRNA locus (Supplemental Data S1).

Significant, single-nucleotide unambiguous 3′ addition was observed in all libraries above the estimated error rate for adenine and uridine (Fig. 1A; see Methods for details). The proportion of miRNA loci with significant nucleotide addition was consistent across all organisms and cell lines (Fig. 1A). Strikingly, a subset of miRNA loci appears to be frequently targeted for significant adenine and uridine addition in mammals (Fig. 1B,C; Supplemental Table S1). This occurred regardless of the miRNA expression profile of a cell type and membership in the subset is not dependent on level of miRNA expression, as the extent of addition and level of

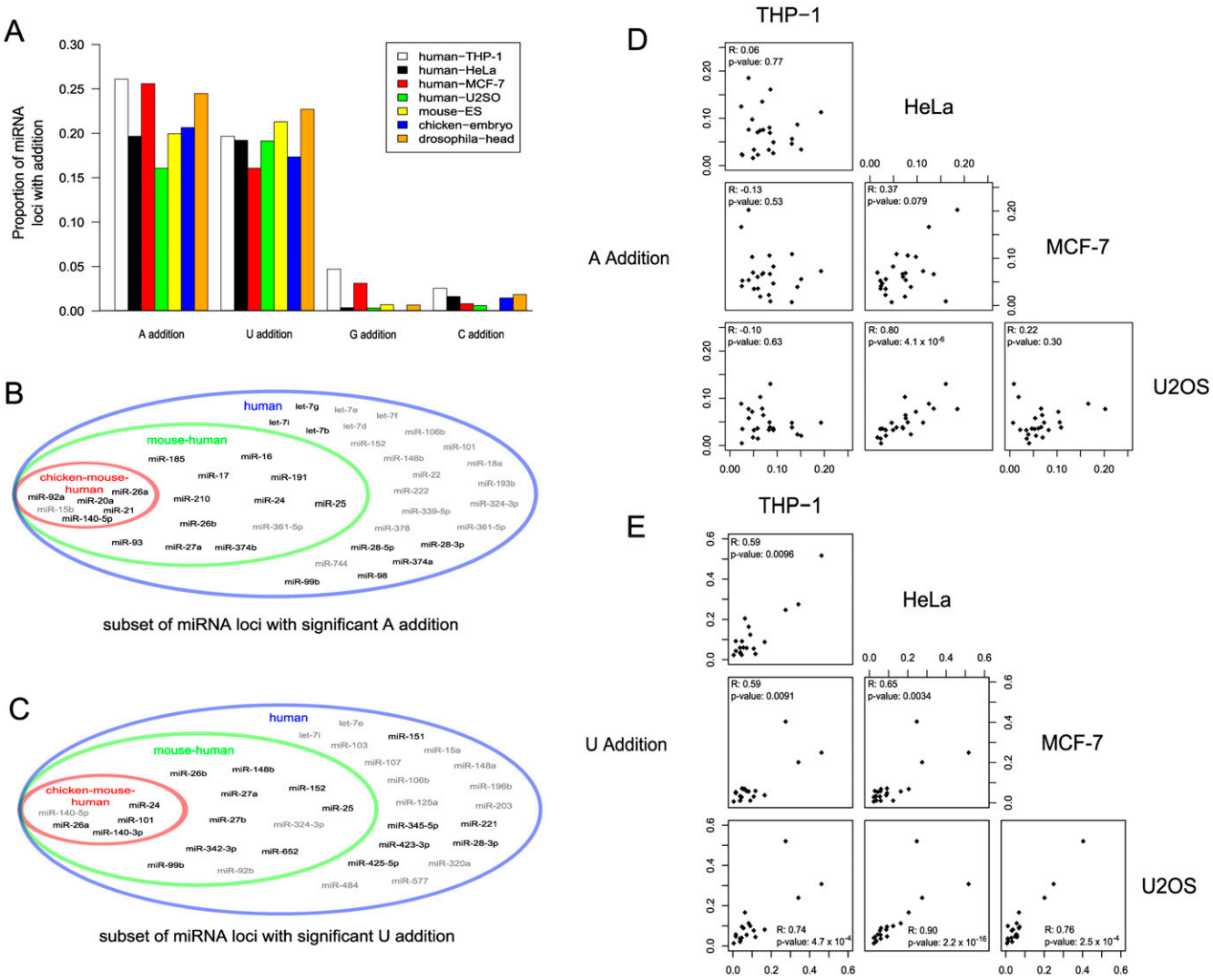

Figure 1. 3′ miRNA addition across organisms. (*A*) Proportion of miRNA loci found to have single nucleotide unambiguous addition significantly greater than expected error rate (see Methods) across seven deep-sequenced short RNA libraries in four species. Sets of miRNA loci with adenine addition (*B*) and uridine addition (*C*) found to have significant amounts of addition in multiple vertebrate species. miRNA loci shaded in gray have significant addition in three of the four human cell lines; loci shaded in black have significant addition in all four human cell lines. Comparison of the proportion of unambiguous adenine (*D*) and uridine (*E*) addition for individual miRNA loci in the four human cell lines; Spearman's correlation and *P*-values are given in the corners of individual scatterplots.

expression were not correlated (see Supplemental Fig. S1; Table S2). Despite being an incomplete picture of miRNA addition, as miRNA with high levels of addition can be expressed only in specific cell types (Katoh et al. 2009), these observations suggest that some miRNAs are more likely to be targeted for addition than others. Similar subsets of miRNA loci were not observed for cytidine or guanine 3′ addition, while *Drosophila* did not have adenine or uridine addition at homologous miRNA loci. The proportions of adenine and uridine addition at individual miRNA loci are strongly correlated across different libraries constructed from THP-1 cells (see below). Interestingly, comparison of the percentage of addition in the same miRNA loci across all analyzed human cell lines revealed consistent correlation for uridine addition, but not for adenine addition (Fig. 1D,E; Supplemental Table S3). While this analysis encompasses only four cell types, it hints at the possibility that adenine addition at miRNA loci fluctuates across cell types while uridine addition occurs at similar rates.

Significant, double-nucleotide unambiguous 3′ additions were also observed. Unexpectedly, several combinations of unambiguous double nucleotide addition events were observed in high numbers, including AA and UU addition across all organisms and cell types and AU, UA, and possibly AG in human and mouse tissues (Supplemental Table S4). This suggests that mammals may have several distinct and repeatedly occurring 3′ miRNA modification types.

Global effects of miRNA nucleotidyltransferase knockdown

Three different members of the TRF family of nucleotidyltransferases were selected for siRNA-mediated knockdown: the PAPD4, PAPD5, and PAPD7 (formerly known as POLS) enzymes. These enzymes were selected based on several criteria: prior experimental evidence, expression in the THP-1 cell line (The FANTOM Consortium and the Riken Omics Science Center 2009; Severin et al. 2009), and careful reconstruction of the evolutionary depth of the various TRF subfamilies which was subsequently aligned with the previously reconstructed depth of the animal miRNA biogenesis machinery in the cell (Supplemental Methods; Supplemental Tables S5, S6; Supplemental Fig. S2; Anantharaman et al. 2002; Grimson et al. 2008; Muljo et al. 2009).

The frequency of unambiguous adenine addition was clearly reduced across a large spectrum of miRNA loci in the PAPD4 knockdown while remaining unchanged in the PAPD7 library and displaying limited reduction in the PAPD5 library (Fig. 2A); other additions also saw similar, broadly observed PAPD4-mediated

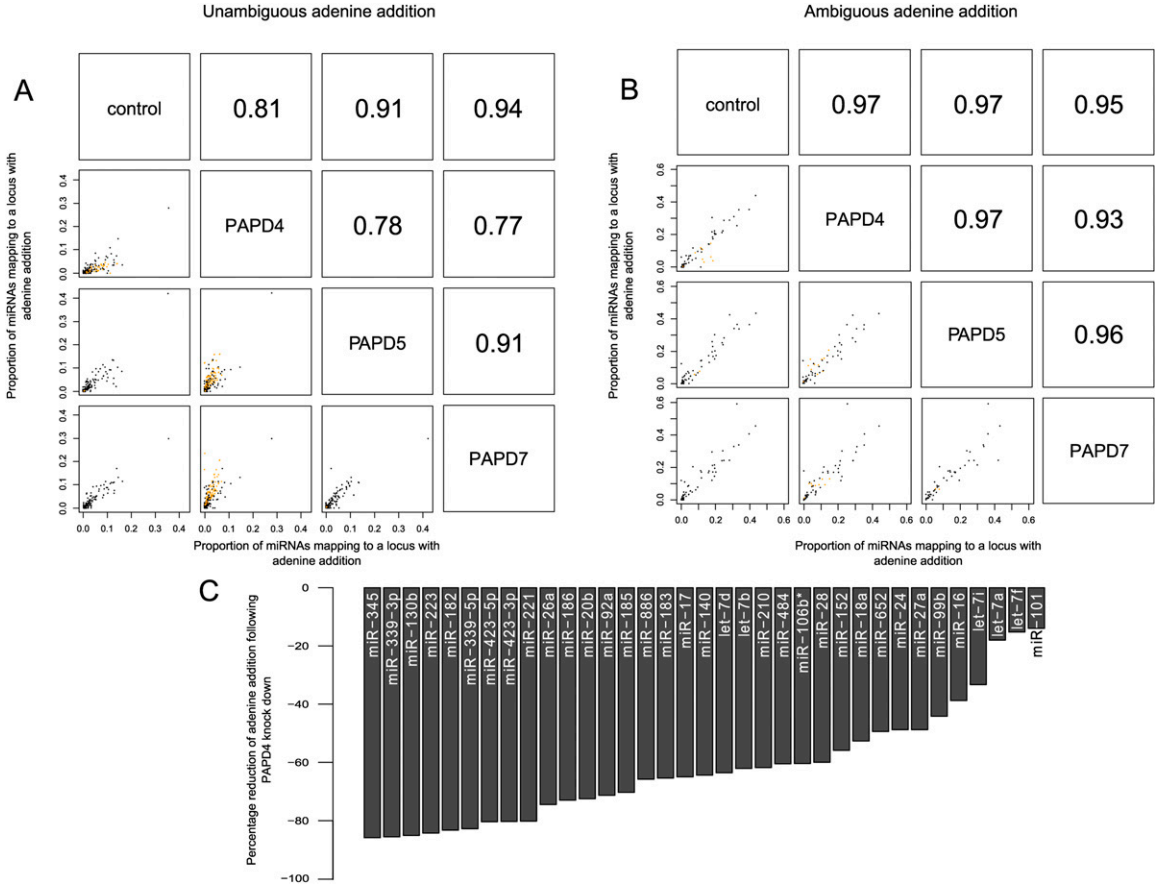

Figure 2. PAPD4 broadly affects adenine addition at THP-1 miRNA loci. Comparison of unambiguous adenine addition rates (*A*) and ambiguous adenine addition rates (*B*) across control and PAPD4, PAPD5, and PAPD7 knockdown short RNA libraries. *Lower left* panels plot the percentage of adenine addition at specific loci between libraries, which are labeled on the diagonal panels. Loci with <50 sequence tags in the control condition are excluded to reduce noise. *Upper right* panels give the Pearson's correlation between two libraries. Loci with significant decrease (Fisher's exact test, Bonferroni post hoc correction) in addition relative to control library are colored in orange. (*C*) Percentage of reduction in adenine addition at miRNA loci in the PAPD4 knockdown library relative to control library for miRNA loci which meet the following two requirements: (1) reduction relative to control library is significant, and (2) addition is significantly greater than the expected error rate of addition (see Methods).

reductions in addition including AA, AU, G, and GA (Supplemental Figs. S3–S8; Supplemental Table S7). Widespread reduction in ambiguous addition was not observed in any library (Fig. 2B; Supplemental Figs. S9–S14; Supplemental Table S8), suggesting that differential endonuclease-mediated cutting is also a significant contributing factor to miRNA 3′ end variation.

Single, unambiguous adenine addition was significantly reduced in 31 of the 73 (42%) miRNA loci containing unambiguous adenine additions above the estimated sequencing error rate in the PAPD4 knockdown library, with 71 (97%) loci showing at least some reduction. The total percentage drop in tags containing a significant unambiguous adenine addition ranged between 14% and 100% (Table 1; Fig. 2A,C; Supplemental Table S9). Four of the 35 loci (11%) with ambiguous adenine additions above the estimated sequencing error rate also exhibited significant PAPD4-mediated reductions (Table 1; Fig. 1B,C; Supplemental Table S9), with 19 (54%) loci showing at least some reduction. Included among PAPD4-targeted miRNAs are many members of the paralogous polycistronic gene clusters *mir-106a-92*, *mir-106b-25*, and *mir-17-92* (Table 1; Petrocca et al. 2008a), which have been implicated in various processes relating to development and tumorigenesis (Ivanovska et al. 2008; Koralov et al. 2008; Petrocca et al. 2008b; Ventura et al. 2008; Xiao et al. 2008). This, in addition to the targeting of other miRNAs linked to similar processes including miR-221 (le Sage et al. 2007), miR-16 (Cimmino et al. 2005), miR-24 (Lal et al. 2009), and let-7 (Mayr et al. 2007), suggests that PAPD4 and 3′ adenine addition could affect cell cycle progression and tumorigenesis, consistent with a previously determined role for PAPD4 in controlling cell cycle (Wang et al. 2002).

Unambiguous, single guanine addition was also significantly reduced in the PAPD4 library in eight of the 13 miRNA loci with additions above the estimated sequencing error rate (Supplemental Tables S7, S9). We also identified miRNA loci with significant reductions in uridine addition in the PAPD5 knockdown library

Table 1. miRNA loci targets of PAPD4 adenylation in THP-1, their conservation across species, and percentage change of adenylation when associating with different AGO proteins

miRNA loci name	Percentage reduction PAPD4 KD[a]	Human addition	Mouse addition	Chicken addition	*Drosophila* addition	Percentage reduction EIF2C1	Percentage reduction EIF2C2	Percentage reduction EIF2C3
Unambiguous adenine addition								
hsa-let-7a	−16.2	Δ		o	o[b,c]	+8.6[a]	−24.2[d]	−47.7[d]
hsa-let-7b	−60.3	o		o	—	+6.2	−10.9[d]	−21.1[a]
hsa-let-7d	−63.7	Δ		o	—	+2.8	−22.6[d]	−51.1[d]
hsa-let-7f	−13.7	Δ		o	—	−6.1	−30.5[d]	−55.8[d]
hsa-let-7i	−32.1	o		o	—	−38.1[d]	+0.3	−37.1[d]
hsa-miR-106b*	−61.0	Δ		n	n	−13.9	−39.9	−58.7
hsa-miR-130b	−85.0	Δ	o	o	n	−23.1	−61.2[d]	−6.2
hsa-miR-152	−55.6	Δ		n	n	+24.2	+0.5	−15.4
hsa-miR-16	−38.8	o	o		n	+32.5[a]	−23.1[d]	−32.8[d]
hsa-miR-17	−64.9	o	o		n	−13.8	−35.5[d]	−42.4[d]
hsa-miR-182	−83.4	Δ	o	n	n	+66.9	+83.6	−39.3
hsa-miR-183	−63.5	Δ	o		n	−36.1	−50.2[d]	−60.4[d]
hsa-miR-185	−70.3	o	o	n	n	+61.5[a]	−12.9	−11.2
hsa-miR-186	−72.5	o	o	n	n	−65.1[d]	−56.4[d]	−64.2[d]
hsa-miR-18a	−53.3	o			n	−35.8	−21.6	−37.2
hsa-miR-20b	−72.0	Δ	o	o	n	+35.4	+7.1	−42.3
hsa-miR-210	−57.5	o	o	n	o	+21.4	−13.8	−13.4
hsa-miR-223	−83.5	Δ		o[b]	n	−7.8	−53.7[d]	−69.8[d]
hsa-miR-24	−48.8	o	o		n	+63.0[a]	−19.5[d]	−17.7[d]
hsa-miR-26a	−74.5	o	o	o	n	+19.1	−20.8	−52.2[d]
hsa-miR-27a	−47.3	o	o	n	n	+5.9	−3.9	−38.6[d]
hsa-miR-28-3p	−58.5	o		n	n	−35.7	−54.9[d]	−65.3[d]
hsa-miR-339-3p	−85.3	Δ		n	n	+23.6	−38.2	−12.3
hsa-miR-339-5p	−81.5	o		n	n	−28.6	−13.6	−45.6
hsa-miR-345	−85.8	Δ		n	n	+11.9	−57.9[d]	−61.6
hsa-miR-423-3p	−80.3	o		n	n	+15.4	−29.7[d]	−62.8[d]
hsa-miR-423-5p	−81.3	o		n	n	+39.8[a]	−2.0	−12.1
hsa-miR-652	−49.4	Δ		n	n	+0.7	+6.8	+3.0
hsa-miR-886	−66.0	Δ	n	n	n	−37.8	−51.9	−50.1
hsa-miR-92a	−71.3	o	o	o		+1.1	−1.5	−28.5[d]
hsa-miR-99b	−42.8	o		n	n	−38.9	−30.3	−55.6[d]
Ambiguous adenine addition								
hsa-miR-101	−12.6	o[b]		o	n	+27.5	−38.4[d]	+16.9
hsa-miR-140-3p	−62.2	o[b]	o[b]	o	n	−17.8	−32.3[d]	−57.9[d]
hsa-miR-221	−77.1	Δ[b]		o	n	+48.7	−13.0	+17.6
hsa-miR-484	−61.5	Δ[b]	o[b]	n	n	+23.8	−6.8	+14.1

(o) Significant adenine addition observed; (Δ) significant adenine addition observed in either THP-1 or HeLa cells; (n) no clear homology with the human miRNA loci in the organism.
[a]Significant increase in adenine addition.
[b]Observed addition in organism is ambiguous.
[c]Only one let-7 ortholog is present in *Drosophila*.
[d]Significant reduction in adenine addition.

(Supplemental Tables S8, S10), while the PAPD7 knockdown library notably contained little or no significant reductions. Taken together with the recent identification of the ZCCHC11 enzyme as an uridylating enzyme which targets miR-26a (Jones et al. 2009), this result suggests that multiple nucleotidyltransferases are involved in 3′ miRNA uridine addition in the cell.

We next compared the miRNA targets of PAPD4 single adenine addition to the subset of miRNA loci with significant adenine additions identified above (Table 1). Twenty-nine out of the 35 (83%) miRNA loci regulated by PAPD4 in THP-1 cells have conserved, significant adenine addition in at least one other library analyzed. Additionally, three of the six miRNA loci comprising the subset of miRNAs with adenine addition across all analyzed vertebrate short RNA libraries are targeted in THP-1 by PAPD4, and nine of the 20 (45%) loci with significant addition in both human and mouse are targeted in THP-1 by PAPD4 (Fig. 1B; Table 1). These observations suggest PAPD4 often targets the subset of miRNA loci consistently subjected to adenine addition across different cell lines.

Affects of adenine addition on stability and mRNA target expression

If PAPD4-mediated adenine addition contributes to miRNA stability as previously proposed (Katoh et al. 2009; Kai and Pasquinelli 2010), we expected to see reduced total counts in at least a subset of miRNAs after PAPD4 knockdown. We analyzed the effect of different nucleotidyltransferase knockdowns on total miRNA counts across individual miRNA loci. Correlation between total miRNA counts was extremely high in the PAPD4 knockdown library (Fig. 3A) as well as the other nucleotidyltransferase knockdown libraries (Supplemental Fig. S15; Supplemental Table S11), suggesting that PAPD4-mediated adenine addition does not globally affect the stability of miRNA. We next tested whether mRNA expression of known targets might be affected by adenine addition. Expression of the *ZBTB10* gene, a target of miR-27a (Scott et al. 2006) expressed in THP-1, was tested by transfecting the mimic miRNA duplex sequences as well as a version of the miRNA with a single adenine addition. Addition of a single adenine to the 3′ end of the miRNA reduced repression of the target mRNA, although given that the reduction was just outside the realm of statistical significance ($P = 0.065$) caution should be used in interpreting these results (Fig. 3B). Several predicted targets of miR-26a known to be expressed in THP-1 were also tested. The *CHORDC1* gene was identified as a novel target of miR-26a and *SMAD1* mRNA levels were also repressed by miR-26a in THP-1 (Luzi et al. 2008). Again, repression of the target mRNAs was reduced by the adenylated miRNA. Significant differential expression for these two targets were observed at $P < 0.05$ (Fig. 3C,D).

We also tested the expression level of mRNA known to be targets of miRNA substrates of PAPD4-mediated adenine addition

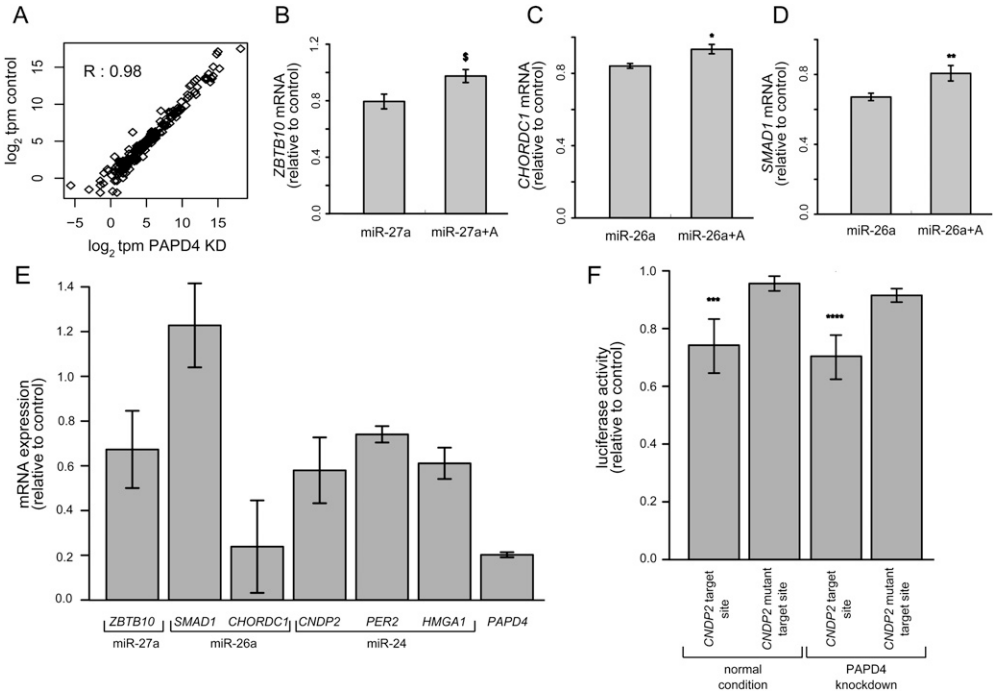

Figure 3. miRNA expression levels are unaffected by PAPD4 knockdown and 3′ miRNA adenine addition reduces mRNA target repression. (*A*) Total sequence tag counts mapping to all miRNA loci compared across the control and PAPD4 knockdown short RNA libraries. Tag counts are normalized into tags per million (tpm) and $\log_2$-transformed. Pearson's correlation is given in the *upper left* corner of the plot. (*B–D*) Targets of miRNA (*B*, *ZBTB10*; *C*, *CHORDC1*; *D*, *SMAD1*) are repressed after transfection of primary miRNA sequence (*left*) and repression is reduced after transfection of miRNA with 3′ adenine addition (*right*). Expression ratio is normalized to the endogenous *GAPDH* mRNA level, with average values bracketed by SEM error bars (Methods). While *ZBT10* expression appears to be reduced, the change is not significant at a threshold $P < 0.05$. $^{\$}P = 0.065$ for miR-27a targeting of *ZBTB10*, $^{*}P = 0.030$ for miR-26a targeting of *CHORDC1*, and $^{**}P = 0.028$ for miR-26a targeting of *SMAD1* (paired Students *t*-test, $n = 3$). (*E*) Expression levels of mRNA targets of different miRNA are generally decreased after knockdown of PAPD4. Each bar represents a distinct mRNA target, labeled on the *x*-axis along with the known miRNA that targets that gene. Expression ratio is normalized as in *B–D*, with $n = 4$. The expression level of *PAPD4* during knockdown is provided as a reference in the *far right* bar of the plot. (*F*) Luciferase activity of reporter assay for wild-type and mutated miRNA target sequence of *CNDP2* mRNA transcript. Luciferase activity is measured as described in Methods and tested in normal and PAPD4 knockdown conditions. $^{***}P = 0.035$ in normal condition and $^{****}P = 0.015$ in PAPD4 knockdown condition (paired Students *t*-test, $n = 4$).

in THP-1 cells subjected to PAPD4 knockdown (Fig. 3E). As knockdown of PAPD4 affects many miRNA loci at the same time and possibly the mRNA transcripts themselves (Suh et al. 2006; Benoit et al. 2008), the expression of the target mRNA could be affected by downstream effects resulting in unclear results. Nevertheless, we observed a tendency for the mRNA targets to have significantly reduced expression following PAPD4 knockdown (Fig. 3E). Previous experiments showed an increase in expression of mRNA targets of miR-122 following knockout of PAPD4 in mouse liver (Katoh et al. 2009). However, here we are measuring expression of transcripts previously determined to be targeted at the mRNA level by miRNA (Scott et al. 2006; Lal et al. 2009;) and these same miRNA loci are substrates of PAPD4 in THP-1 cells (Table 1). Further discussion of these results, including the unusual increase in *SMAD1* expression (Fig. 3E), can be found in the Supplemental Material.

To further probe the interplay between adenine addition and miRNA targeting effectiveness, we constructed plasmids with the miRNA target sequence of the *CNDP2* gene and a mutated version of the target sequence fused to a luciferase reporter gene. Luciferase activity was significantly ($P < 0.05$) reduced in the plasmid containing the miRNA target sequence relative to a negative control lacking an insertion and the plasmid containing the mutated target sequence (Fig. 3F). We also tested the same plasmids following siRNA-mediated PAPD4 knockdown. Luciferase activity in this condition was consistently reduced relative to the normal condition, again suggesting a reduction in adenine addition reduces expression of the miRNA-targeted gene. The same experiments were performed for plasmids containing miRNA target sequences of the *CHORDC1* gene. Significant reduction relative to the negative control was observed, with the reduction stronger in the PAPD4 knockdown condition (Supplemental Fig. S16).

Adenine addition in AGO-bound miRNA

Reduced effectiveness of adenylated miRNA in repressing target expression coupled with possible increased effectiveness when knocking down PAPD4 led us to speculate that 3′ addition could influence incorporation into the AGO proteins. AGO proteins directly bind miRNA resulting in formation of the RISC, enabling the miRNA to bind target mRNA during RNA-mediated gene repression (Hutvagner and Simard 2008). We performed IP pull-down experiments with the EIF2C1 (also known as AGO1), EIF2C2 (also known as AGO2), and EIF2C3 (also known as AGO3) proteins with cell extract derived from THP-1 cells (Methods) and deep-sequenced short RNA extracted from these experiments alongside a control short RNA sample extracted from the entire cell. We tallied total ambiguous and unambiguous additions as described above (Supplemental Data S2). miRNA bound to the EIF2C2 and EIF2C3 proteins had a reduced number of overall unambiguous adenine additions relative to miRNA extracted from the complete cell (EIF2C2, 25%; EIF2C3, 41%), although reduction in miRNA bound to EIF2C1was less dramatic (9.3%) (Fig. 4). Examination of individual miRNA loci with single, unambiguous adenine addition above the estimated error profile showed some reduction of 3′ adenylation relative to control in 66 of 76 (87%) loci in the EIF2C2 library with 26 (34%) of these statistically significant. Sixty-seven of 76 loci (88%) showed some reduction in the EIF2C3 library with 29 (38%) statistically significant. In contrast, some reduction was observed in only 39 of 76 loci (51%) in the EIF2C1 library with just seven (9%) showing significant reduction while six showed significant increase (8%) (Fig. 4; Supplemental Tables S12, S13). Additional computational analyses were performed to rule out the possibility of a general exonuclease activity being present in the AGO IP-generated libraries (Supplemental Fig. S17). We reasoned that miRNA loci identified above as affected by PAPD4-mediated adenine addition would show reduction. Indeed, specific examination of these loci revealed that reduction was common in both

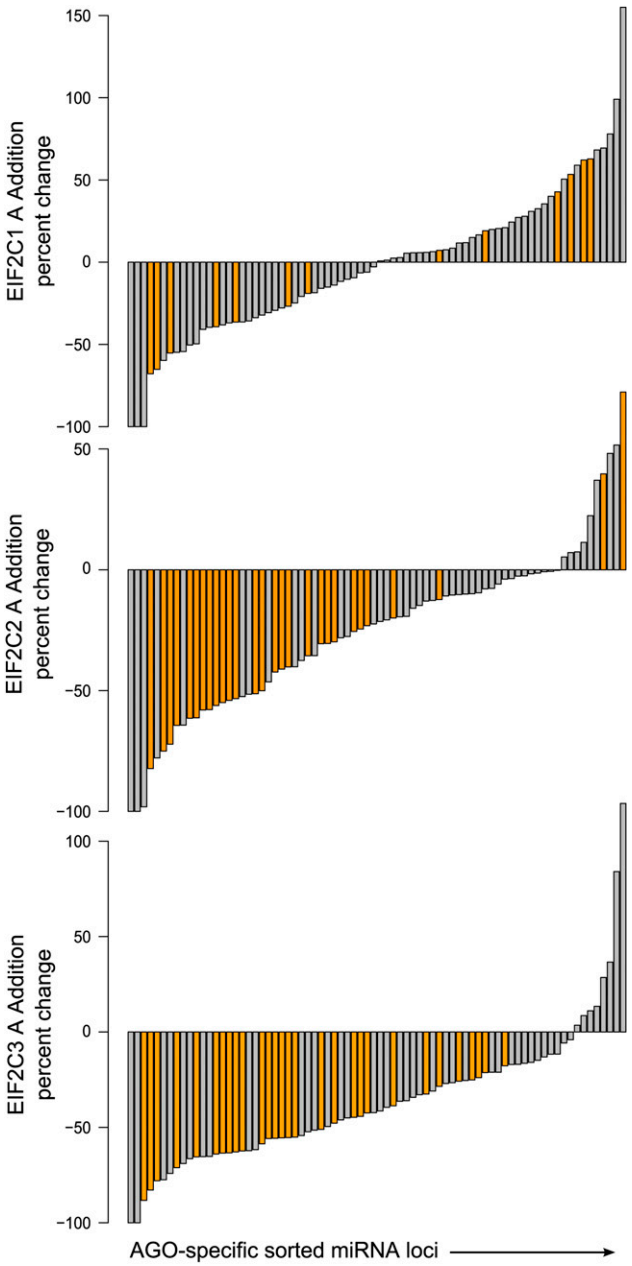

Figure 4. Unambiguous adenine addition is reduced in miRNA bound to EIF2C2 and EIF2C3 proteins. Seventy-six miRNA loci contained significant amounts of 3′ unambiguous adenine addition in the control library. The percentage change of addition in these loci across the EIF2C1, EIF2C2, and EIF2C3 libraries are depicted as barplots with each bar representing one of the 76 loci. Loci are sorted by order of increasing percentage change; therefore, a bar in one plot does not necessarily represent the same miRNA locus as the corresponding bar in another plot. For the list of miRNA loci with names and percentage reductions, please see Supplemental Tables S12, S13. Bars corresponding to loci with significant reduction or increase in the AGO libraries are colored orange.

the EIF2C2 and EIF2C3 libraries, but surprisingly not in the EIF2C1 library (Table 1). Taken together, these results suggest that 3′ adenine addition to miRNAs (including addition of two adenines) may play a role in reducing the ability of miRNA to interact with EIF2C2 and EIF2C3 proteins, while interaction with EIF2C1 appears to be unaffected by adenine addition. EIF2C2 is the only Argonaute protein in humans with demonstrated endonuclease activity (Liu et al. 2004; Meister et al. 2004). Adenine addition may therefore lessen the likelihood of target mRNAs undergoing regulation via endonuclease "slicer" activity, consistent with the expression data presented here (Fig. 3).

Interestingly, other addition types displayed little general or significant miRNA loci-specific reduction in the different AGO pull-down libraries. Some reduction is observed for uridine addition at individual miRNA loci across the three AGO proteins; however, much of this reduction occurs in instances of ambiguous addition and thus may or may not be related to nucleotidyltransferases acting on 3′ ends of mature miRNA (Supplemental Table S12). In general, these observations suggest that adenylation might specifically be involved in the interaction between miRNA and AGO proteins, while other 3′ addition types are involved in distinct functional roles.

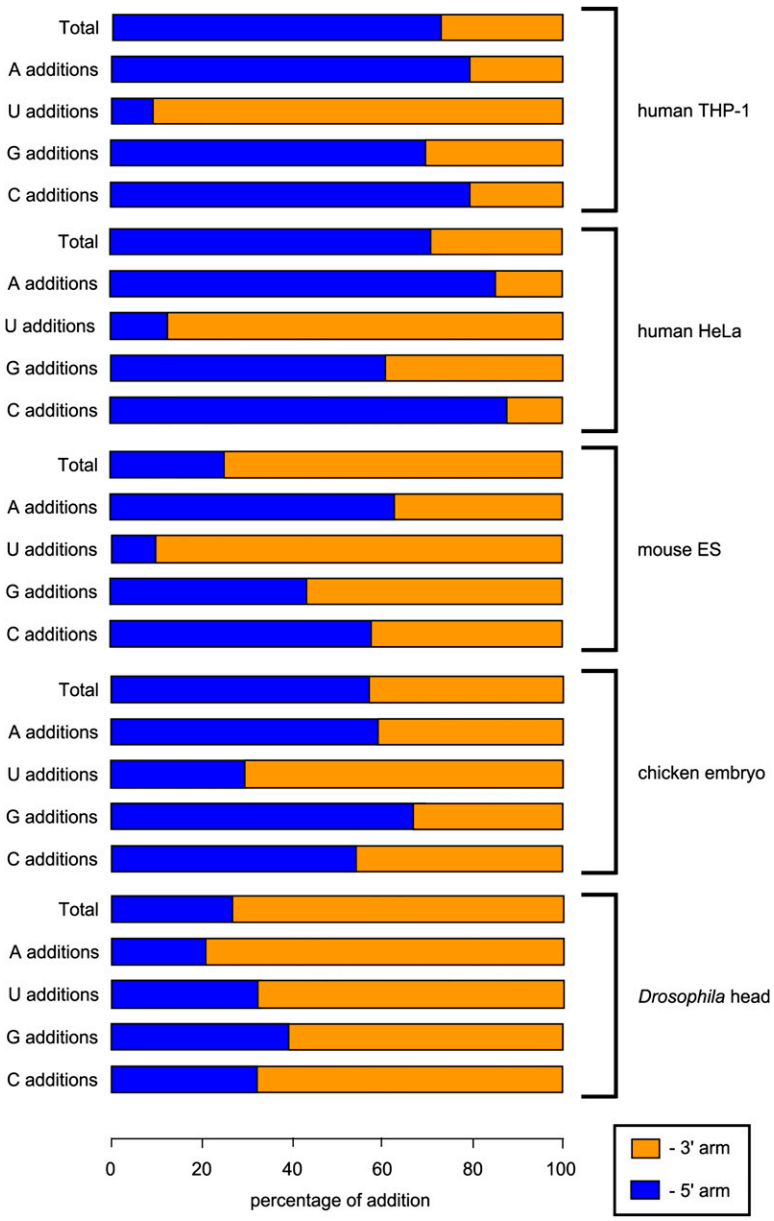

Figure 5. Unambiguous uridine addition occurs predominantly in miRNAs derived from 3′ arm of precursor miRNA. Percentages of unambiguous additions for each single nucleotide are colored according to which arm of the precursor miRNA the addition event originates from. Uridine addition bias is observed across all analyzed vertebrate libraries, species and tissue are labeled on the *right*.

Distribution of 3′ addition across mature miRNA derived from 5′ and 3′ pre-miRNA arms

Recently, multiple uridine additions at the 3′ end of pre-miRNA were shown to block uptake into the DICER1 enzyme (Heo et al. 2009). DICER1 processes pre-miRNA following nuclear export through excision of the characteristic hairpin region (Han et al. 2006). As this parallels the proposed adenine addition function for influencing interaction with AGO proteins, we looked at the distribution of all single nucleotide addition types across mature miRNA derived from the 5′ and 3′ arms of the pre-miRNA in all organisms and tissue types described above, cognizant that addition to a mature miRNA derived from the 5′ arm or the pre-miRNA must necessarily occur after DICER1 processing. We observed that while adenine, cytidine, and guanine addition follow the expected distribution of addition based on total tags derived from the 5′ or 3′ arms, uridine addition showed a dramatic bias in vertebrates, but notably not in *Drosophila*, in favor of addition to mature miRNAs derived from the 3′ arms of pre-miRNA (Fig. 5). The uridine additions observed in this study may therefore be vestiges of addition to the 3′ end of the pre-miRNA that did not accumulate a long enough "uridine tail" to block DICER1 association (Hagan et al. 2009; Heo et al. 2009; Lehrbach et al. 2009).

To assess the global extent of modifications at the 3′ end of precursor miRNA, we analyzed publicly available data sets generated during the FANTOM4 project that deep-sequenced RNA of length 42–82 nt (Taft et al. 2009; De Hoon et al. 2010). While the library is largely composed of tags mapping to tRNA loci, we were able to extract several tags that mapped to precursor miRNA loci (Supplemental Data S3). Despite low tag counts at individual loci, we observed several instances of unambiguous 3′ uridylation and adenylation (Supplemental Fig. S18), indicating that addition events are widespread before DICER1 processing. While PAPD4 localizes to the cytoplasm in *Caenorhabditis elegans*, *Drosophila melonogaster*, and *Xenopus laevis* (Wang et al. 2002; Barnard et al. 2004; Kwak et al. 2008), in mammals it has also been found to

localize to the nucleus (Nakanishi et al. 2006). This might indicate that PAPD4, in addition to acting on post-DICER1 processed miRNA, is also active on precursor miRNA 3′ ends. Alternatively, an as yet unidentified transferase might be adenylating precursor miRNA in the nucleus.

Structural basis for selection of miRNA adenylation substrates

A preference for adenylation of mature miR-122 relative to, but not exclusive to, the miR-122/miR-122* duplex in vitro was previously reported (Katoh et al. 2009). We were unable to identify any characteristic distinguishing the set of single-stranded miRNAs targeted for adenylation from those not targeted for adenylation, including position-specific nucleotide bias or overrepresentation of a motif or set of motifs. Because addition is reduced in miRNA bound to EIF2C2 and EIF2C3 proteins, we speculated that in vivo addition may occur after DICER1 processing but before strand separation, a process occurring after duplex interaction with AGO proteins (Matranga et al. 2005; Rand et al. 2005; Forstemann et al. 2007; Tomari et al. 2007) relying on a set of established structure-based rules in *Drosophila* (Kawamata et al. 2009) and humans (Yoda et al. 2010). This raises the possibility that structural features of the post-DICER1 processed miRNA duplex could influence selection of substrates for adenylation or uridylation.

We calculated pairing probabilities at each nucleotide position for human and mouse miRNA from the subset of miRNA that displayed significant adenylation across the multiple examined cell lines in the analysis from Figure 1 and all human and mouse miRNA that tend to not be subjected to significant adenylation in the same cell lines (Fig. 6A; see Methods). The miRNAs included in this analysis were filtered to remove star sequences to avoid comparison of secondary structural features important in selection of the mature sequence (for complete list of miRNA loci used, see Supplemental Table S14). We observed differences in abundance of tags across the two subsets of miRNA (Supplemental Fig. S19); however, relative abundance does not appear to be related to pairing probability (Supplemental Fig. S19) or addition (Supplemental Fig. S1), suggesting this is not a contributing factor to observed differences. Significant structural differences are observed ($P < 0.05$) discriminating between the two sets of miRNA in both human and mouse sequences (Fig. 6B). When viewed from the perspective of the strand that receives an adenine addition, positions 5, 7, and 19 are more likely to be paired in the duplex structure. The difference in position 19 is of particular interest, as it indicates that a greater double-stranded character at the end of the duplex and near the site of addition may play a role in the selection criteria for adenine addition (Fig. 7). The PAPD4 protein lacks an RNA binding domain, which indicates that an additional cofactor with a double-stranded RNA binding domain may be essential for PAPD4 to interact with its substrate miRNA. Differences in secondary structure as a criterion for selection of adenylation targets is reminiscent of the identification of structural properties as a driving factor in strand selection during miRNA loading of *Drosophila* AGO proteins (Tomari et al. 2007; Kawamata et al. 2009; Ghildiyal et al. 2010). Interestingly, the same analysis for uridylation failed to identify structural differences between the two sets (Fig. 6C,D), perhaps related to the bias for addition in miRNAs derived from the 3′ arm of the pre-miRNA (see above; Fig. 5).

Discussion

The conservation of adenylation and uridylation events at individual miRNA loci across different species indicates that 3′ miRNA addition represents an important post-transcriptional processing event. The data presented here support a role for 3′ adenine addition in attenuating the effectiveness of specific miRNA by interfering with key post-transcriptional events during the miRNA life cycle, similar to different classes of so-called "miRNA assassins" (Kai and Pasquinelli 2010). Typically, only a small fraction (0% to ~20%) of miRNAs derived from a miRNA locus are subject to 3′ adenine addition. Addition could therefore provide a means for the cell to fine-tune the targeting efficiency of the transcripts derived from specific miRNA loci. Intriguingly, the observation that proportions of adenine addition in miRNA loci, in contrast to proportions of uridine addition, are typically not conserved across different cell lines could indicate that such fine-tuning of miRNA efficiency is controlled in a cell type–specific manner (Fig. 1D,E).

The known and proposed consequences of 3′ addition are outlined in Figure 7. Uridylation, at least in part catalyzed by the ZCCHC11 nucleotidyltransferase, primarily occurs on the pre-miRNA and blocks uptake into DICER1. Adenylation, on the other hand, is likely primarily mediated by the PAPD4 enzyme after DICER1 processing. Computational analysis indicates position-specific binding character of the miRNA/miRNA* duplex is a possible criterion in selection of adenylation targets. Adenylated miRNA is reduced in EIF2C2 and EIF2C3 proteins, suggesting adenylation modulates miRNA uptake into the RISC and differential loading of AGO proteins. As such, adenylation could lessen ability of miRNAs to regulate cleavage through the "slicer" activity of EIF2C2 (Liu et al. 2004; Meister et al. 2004). We were unable to detect stable binding between the AGO proteins and the PAPD4 enzyme (Supplemental Fig. S20). Taken together with the above observations, this suggests that PAPD4 adenylates miRNA sometime after DICER1 processing but before strand uptake into the RISC (Fig. 7).

It is important to note that ZCCHC11 has also been linked in at least one instance to mature miRNA uridylation, which showed reduction in efficiency of mRNA targeting similar to the data presented here for adenylation (Jones et al. 2009). This suggests that in at least some loci, post-DICER1 uridylation serves a role similar to post-DICER1 adenylation, although the lack of significant reduction in uridylation in AGO-associated miRNA does not support this on a global scale. Instead, much of the observed unambiguous uridine addition in miRNA may be derived from uridylation events on the 3′ arms of precursor miRNA and possibly represent vestiges of uridylation tails which did not grow long enough in length to block DICER1 uptake (Heo et al. 2009; Jones et al. 2009). The observed correlation of uridine addition proportions across cell lines could suggest that formation of uridylation tails is strictly controlled at specific miRNA loci (Fig. 1E).

Deep-sequencing data also suggest that PAPD5, an enzyme with no previously known role, has a limited role in miRNA uridylation. The identification of a third miRNA nucleotidyltransferase suggests that a complex network of transferase enzymes may be acting to regulate miRNA sequences at different points in their life cycle. The observation that several types of distinct double nucleotide events are present in significant quantities at the 3′ ends of miRNA (Supplemental Table S4) suggests we are only beginning to understand the complexity of animal 3′ miRNA modification.

Two lines of evidence suggest that 3′ addition in *Drosophila* miRNA serves a role distinct from that of vertebrates. First, while 3′ addition is clearly present in *Drosophila*, homologous miRNA loci targeted for adenylation and uridylation are largely nonoverlapping with conserved targets in vertebrates. Second, unlike vertebrates, *Drosophila* shows no bias toward uridylation in miRNA derived from the 3′ arm of the precursor miRNA (Fig. 5). This

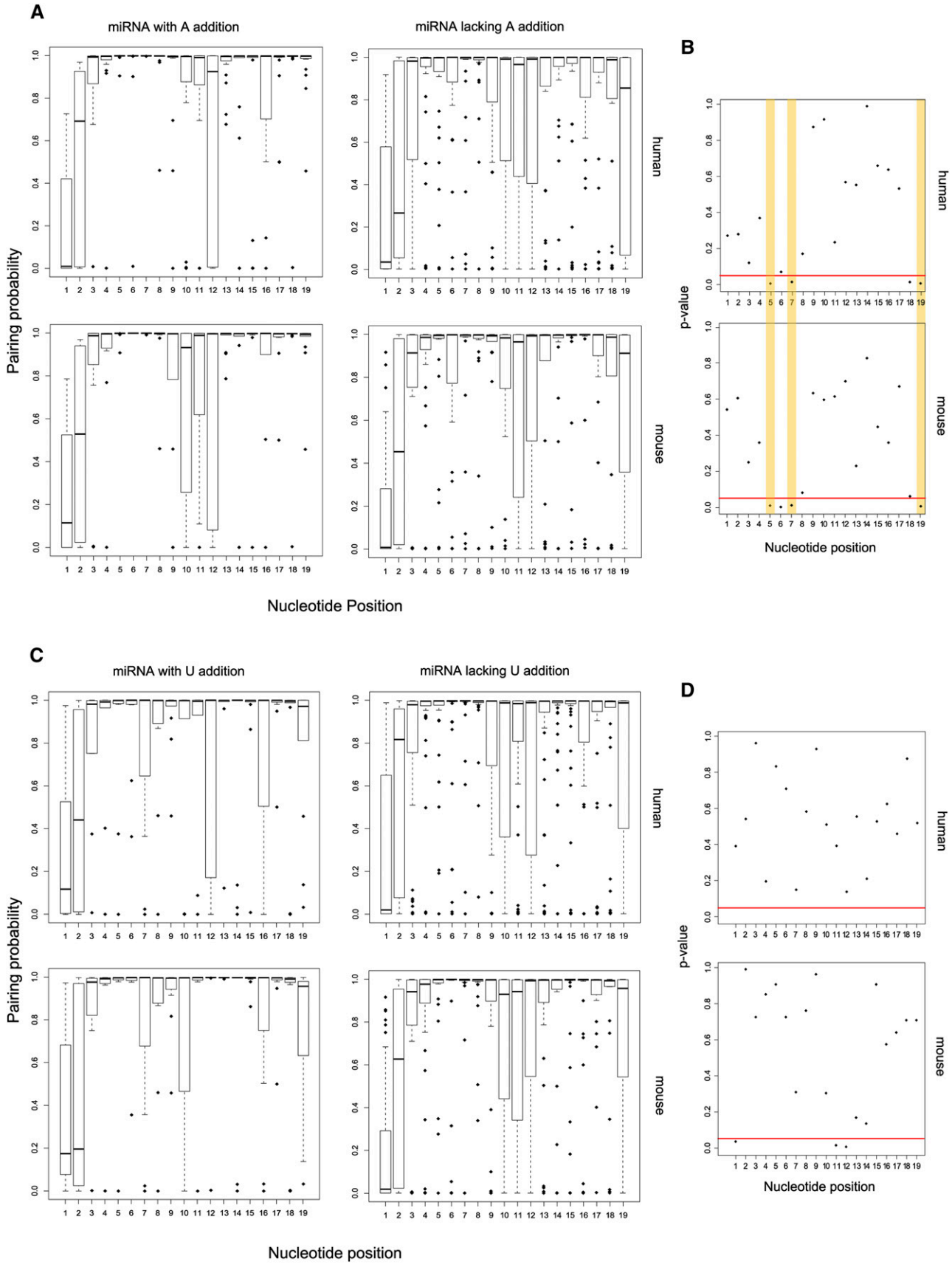

Figure 6. (Legend on next page)

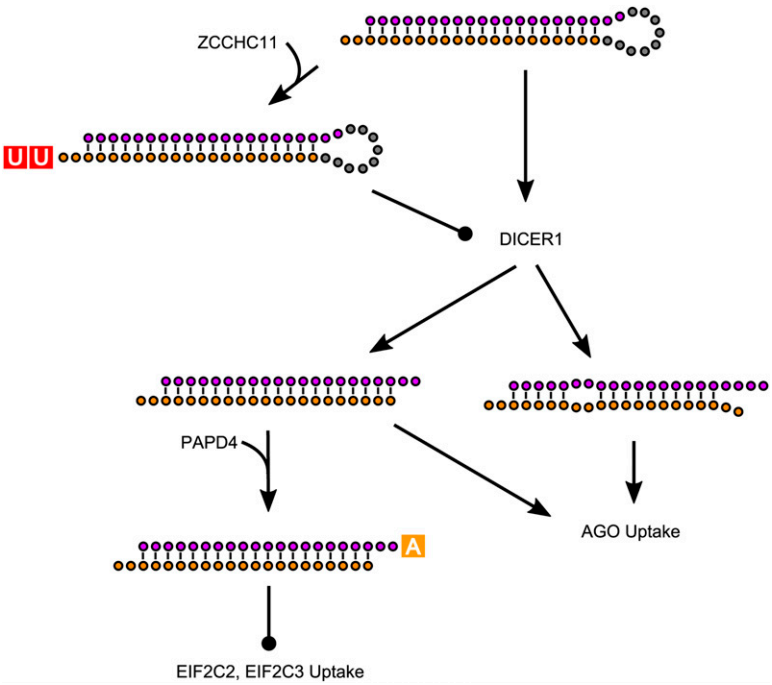

Figure 7. Proposed general mechanism depicting consequences of 3′ addition. Precursor miRNA is depicted with miRNA strands of the processed duplex colored in purple and orange and the hairpin region colored in gray. Formation of uridine tail in precursor miRNA blocks uptake into DICER1, while PAPD4-mediated adenylation of purple strand, predicted to be mediated at least in part by secondary structure character, selectively interferes with uptake into AGO proteins (interactions which are not thought to proceed are depicted with filled circles).

suggests the functional distinction between uridylation of the precursor miRNA and adenylation of post-DICER1 processed miRNA is specific to vertebrates. Thus, analogous to other aspects of miRNA processing including differential loading of strand selection (Ghildiyal et al. 2010) and division of functional roles for paralogous AGO proteins (Hock and Meister 2008), miRNA addition may have divergent roles across distinct monophyletic groups of animals.

Methods

Cell culture, siRNA transfection, RNA extraction, and expression analysis by qRT-PCR

THP-1 cells were cultured in RPMI1640 (Invitrogen), 10% FBS, penicillin/streptomycin (Invitrogen), 10 mM HEPES (Invitrogen), 1 mM sodium pyruvate (Invitrogen), and 50 μM 2-mercaptoethanol (Invitrogen). Reverse transfection of 1×10^6 cells in 60-mm cell culture dish was performed with 20 nM (final concentration) of each siRNA, Opti-MEM (Invitrogen), and 1.6 μg/mL (final concentration) of Lipofectamine 2000 (Invitrogen) according to manufacturer's instructions. Total RNAs were extracted 72 h after transfection with TRIzol (Invitrogen) and FastPure RNA kit (TaKaRa BIO) according to the modified manufacturer's instructions. After phase separation of TRIzol, aqueous phase was mixed with the same amount of 100% ethanol and flowed through a filter cartridge. After RNA binding to the filter cartridge, each bound total RNA was washed three times with 700 μL of treble ethanol diluted wash buffer and eluted with elution buffer. RNA was quantified with NanoDrop (NanoDrop Technologies). All siRNA transfection experiments were performed in biological quadruplicate. For each lot of cells, the siRNA-treated cells that were transfected into two separate dishes were combined to give one lot from which RNA samples were extracted. Expression levels of siRNA target genes in the cells treated with the specific siRNAs or the calibrator negative control siRNA were estimated by qRT-PCR in triplicate with the specific primer sets. The procedures for qRT-PCR were essentially as described (Tomaru et al. 2009), with the expression ratio of the target gene mRNA normalized to endogenous *GAPDH* mRNA levels using the $\Delta\Delta C_T$ method (Livak and Schmittgen 2001). Primer sequences for qRT-PCR and mimic miRNA sequences used for transfection are provided in Supplemental Information.

siRNA sequences

Stealth siRNAs designed by Invitrogen were used for RNAi knockdown of nucleotidyltransferase genes. Three distinct stealth siRNA were tested for RNAi activities against their target gene and the siRNA giving a higher level of knockdown was selected for short RNA library construction. Stealth RNAi Negative Control Medium GC Duplex #2 (Invitrogen) was used as negative control siRNA.

Selected siRNAs were as follows.

PAPD4 5′-AUUACAUGGAGCUUGAUGUACAAGG-3′; 5′-CCUUGUACAUCAAGCUCCAUGUAAU-3′
PAPD5 5′-AACAACGUAGGCAUAAUCAAAGGCC-3′; 5′-GGCCUUUGAUUAUGCCUACGUUGUU-3′
PAPD7 5′-AUGAUCAGUGUUCUGGAAGUGGUGG-3′; 5′-CCACCACUUCCAGAACACUGAUCAU-3′.

Mimic miRNA sequences

Transient dsRNA transfections of THP-1 cells were performed as described above with the annealed miR-27a RNA (5′-UUCACAGUGGCUAAGUUCCGC-3′) and miR-27a* RNA (5′-AGGGCUUAGCUGCUUGUGAGCA-3′) or with miR-27a+A RNA (5′-UUCACAGUGGCUAAGUUCCGCA-3′) and miR-27a* RNA; with the annealed

Figure 6. Pairing probability profiles for miRNA with and without 3′ addition events. (*A*) Boxplots depict the pairing probabilities, and by extension the double-stranded character, of individual nucleotide positions in miRNA at positions 1–19. Boxplots to the *left* depict the double-stranded character of the set of miRNA with significant unambiguous A addition conserved across human THP-1, human HeLa, and mouse embryonic stem cells. Boxplots to the *right* depict double-stranded character of the set of miRNA that never show significant addition across the same cell types. Plots to the *top* are constructed with the sequences of human miRNA; plots to the *bottom* are constructed with the sequences of mouse miRNA. (*B*) *P*-values of Wilcoxon rank sum test comparing pairing probabilities at nucleotide positions 1–19 across miRNA with addition and without addition are plotted. Red line plotted at $P = 0.05$, the level of significance. Positions with conserved significance across human and mouse miRNA are highlighted in yellow. (*C*,*D*) Same as *A*, *B*, but testing the set of miRNAs with conserved unambiguous uridine addition.

miR-26a RNA (5′-UUCAAGUAAUCCAGGAUAGGCU-3′) and miR-26a* RNA (5′-CCUAUUCUUGGUUACUUGCACG-3′) or with miR-26a+A RNA (5′-UUCAAGUAAUCCAGGAUAGGCUA-3′) and miR-26a* RNA. The cells were collected 24 h after transfection and total RNAs were extracted as described above. Mimic miRNAs were phosphorylated at the 5′ end.

Luciferase reporter assay

For construction of a vector containing miRNA target sequence fused downstream from a firefly luciferase expression cassette, we used the pmirGLO Dual-Luciferase miRNA Target Expression Vector (Promega). PCR primers sharing 15 bases (underlined) of homology with the sequence at each end of the XhoI-linearized pmirGLO vector and 26 bases (italicized) complementary with the antisense primer were designed. We made double-stranded DNA by overlap extension PCR using the following primer pairs and cloned into the vector using the In-Fusion Advantage PCR Cloning Kit (Clontech). The insert regions in the vectors were sequenced to verify incorporation of the miRNA target sequence.

CNDP2-miR-24: sense 5′-GCTCGCTAGCCTCGAATTC*GAGAGTTGGAGGCTGCGA**TGAGCCA**T*-3′ and antisense 5′-CGACTCTAGACTCGA*ATGGCTCATCGCAGCCTCCAACTCTC*-3′

CNDP2-miR-24mut: sense 5′-GCTCGCTAGCCTCGAATTC*GAGAGTTGGAGGCTGCGA**TGAAAA**T*-3′ and antisense 5′-CGACTCTAGACTCGA*ATTTTCATCGCAGCCTCCAACTCTC*-3′

The boldface characters show predicted target sequences of miRNA seed or mutated seed sequence.

HeLa cells were cultured in DMEM (Invitrogen), 10% FBS, penicillin/streptomycin (Invitrogen). Transfection of 1×10^5 cells/well in a 12-well cell culture plate was performed with 20 nM (final concentration) of each siRNA, 0.8 μg of each plasmid, Opti-MEM (Invitrogen), and 3 μg/mL (final concentration) of Lipofectamine 2000 (Invitrogen) according to manufacturer's instructions. Cells were collected after 24 h for assay using the Dual-Glo Luciferase Assay System (Promega) as described by the manufacturer. Firefly luciferase activity was normalized to *Renilla* luciferase activity to adjust for variations in transfection efficiency among experiments. The results are presented as a relative response ratio (RRR).

RRR = [(experimental sample ratio) – (background ratio)]/[(control ratio) – (background ratio)]

The empty pmirGLO vector was transfected with siRNA as a control reporter vector (control). Total RNAs were extracted from a part of the same cells used for the assay and checked for the knockdown ratio of the PAPD4 gene. All experiments were performed in quadruplicate with data averaged from at least four independent experiments.

Immunoprecipitation

Immunoprecipitation (IP) of AGO-bound RNAs was performed using microRNA Isolation Kit Human Ago2 (Wako) for EIF2C2 and custom-made microRNA Isolation Kit for EIF2C1 or EIF2C3 (provided by Wako) according to manufacturer's instructions. Each immunoprecipitated AGO protein was detected by Western blotting to check for successful IP using anti-human EIF2C1 (07-599, Upstate), anti-human EIF2C2 (07-590, Upstate), and anti-human EIF2C3 (N-12, Santa Cruz Biotechnology) (Supplemental Fig. S17). PAPD4 was detected using anti-PAPD4 (AV49115, Sigma-Aldrich Co.). Cultured THP-1 cells (1×10^7 cells for EIF2C2 IP; 2×10^7 cells for EIF2C1 or EIF2C3 IP) were collected and incubated in cell lysis solution for 10 min on ice. Cell lysates were cleared by centrifugation at 20,000*g* for 20 min at 4°C. One hundred microliters of anti-human Ago1 antibody beads solution for EIF2C1 IP, 50 μL of anti-human Ago2 antibody beads solution for EIF2C2 IP, and 100 μL of anti-human Ago3 antibody beads solution for EIF2C3 IP were added to each cell lysate and mixed by rotation for 2 h at 4°C. Beads were washed twice with cell lysis solution, and each bound AGO-RNA complex were eluted with elution solution. Eluted complexes were extracted with phenol/chloroform, and RNAs were precipitated with ethanol. Purified immunoprecipitated RNAs were used for construction of short RNA libraries.

Short RNA library construction and Genome Analyzer sequencing

Each 10 μg of total RNA samples were size-fractionated to <30 nt using flashPAGE Fractionator system (Ambion) and the fractionated short RNAs were precipitated with ethanol according to manufacturer's instructions. Purified short RNAs were used for the construction of short RNA libraries.

Short RNA libraries were constructed using Small RNA Sample Prep Kit v1.5 (Illumina) according to manufacturer's instructions. Purified short RNA cDNA libraries were checked for amount and quality using Agilent 2100 BioAnalyzer with a DNA1000 Labchip (Agilent) and sequenced using Genome Analyzer GA-II (Illumina) according to the manufacturer's instructions.

Bioinformatics analysis of short RNA tag libraries

Sequences of the linkers attached during short RNA library construction were computationally removed from the tags extracted from sequencing runs. Artifacts introduced into the library through linker-formed dimers and, where applicable, the introduction of siRNA sequences were removed by the Tagdust program (Lassmann et al. 2009). Sequences were then aligned to the genome allowing for up to two mismatches using the Nexalign program (http://genome.gsc.riken.jp/osc/english/software) (De Hoon et al. 2010). Alignments were further refined through correcting for cross-mapping of sequences that map to multiple loci, which weights the set of all potential mapping sites based on frequency of individual tags and positional error likelihood (De Hoon et al. 2010). Tags mapping to miRNA loci defined by miRBase (Griffiths-Jones et al. 2008) were included in the analysis. To reduce noise, we employed a cutoff of 50 tags per million (tpm) at a miRNA locus for inclusion in all analyses, unless otherwise indicated. We collected the complete set of seed sequences that mapped exactly to a miRNA locus that contained distinct 5′ variations. Any tag which exactly matched a seed sequence and contained a 3′ addition was tallied as either an ambiguous or unambiguous addition. Unambiguous double nucleotide additions were additionally separated into two distinct categories: those which could have arisen via an ambiguous addition followed by an unambiguous addition and those which were clearly unambiguous additions (see Supplemental Data S1–S3 online). Only the latter were considered "true" instances of double nucleotide unambiguous addition and were included in subsequent analyses. Additions were summed across all seed sequences for a given locus; these numbers were used for condition-specific loci comparisons. Differences in additions at each miRNA locus were compared using Fisher's exact test. Differences were considered significant at $P < 0.05$ with a Bonferroni post hoc correction. Loci with addition below the estimated sequencer-associated error rate in the control condition were not included in the analyses. The error rate was taken as the percentage of unambiguous addition of cytidine residues at miRNA loci (which have not been implicated in miRNA 3′ addition events), and loci with significantly more additions than the error rate were determined by employing Fisher's exact

test with a Bonferroni post hoc correction. Pairing probability profiles were constructed essentially as described (Ghildiyal et al. 2010) using the RNAcofold program from the ViennaRNA-1.8.4 package (http://www.tbi.univie.ac.at/RNA/). Given the relative depth of sequencing, the count threshold for inclusion of an miRNA and its predicted cognate strand was 30 tpm instead of 10 tpm and comparisons were performed across the set of miRNA with significant 3′ additions in at least three of the four analyzed human cell lines and mouse ES cells and the set of miRNA lacking significant 3′ additions in at least three of the four analyzed human cell lines and mouse ES cells (see Supplemental Table S14 for lists). Statistical analyses were performed using the R language and environment for statistical computing.

Acknowledgments

This work was supported by a research grant for the Omics Science Center from the MEXT to Y.H.

References

Anantharaman V, Koonin EV, Aravind L. 2002. Comparative genomics and evolution of proteins involved in RNA metabolism. *Nucleic Acids Res* **30:** 1427–1464.

Aravind L, Koonin EV. 1999. DNA polymerase beta-like nucleotidyltransferase superfamily: identification of three new families, classification and evolutionary history. *Nucleic Acids Res* **27:** 1609–1618.

Barnard DC, Ryan K, Manley JL, Richter JD. 2004. Symplekin and xGLD-2 are required for CPEB-mediated cytoplasmic polyadenylation. *Cell* **119:** 641–651.

Benoit P, Papin C, Kwak JE, Wickens M, Simonelig M. 2008. PAP- and GLD-2-type poly(A) polymerases are required sequentially in cytoplasmic polyadenylation and oogenesis in *Drosophila*. *Development* **135:** 1969–1979.

Cimmino A, Calin GA, Fabbri M, Iorio MV, Ferracin M, Shimizu M, Wojcik SE, Aqeilan RI, Zupo S, Dono M, et al. 2005. miR-15 and miR-16 induce apoptosis by targeting BCL2. *Proc Natl Acad Sci* **102:** 13944–13949.

De Hoon MJ, Taft RJ, Hashimoto T, Kanamori-Katayama M, Kawaji H, Kawano M, Kishima M, Lassmann T, Faulkner GJ, Mattick JS, et al. 2010. Cross-mapping and the identification of editing sites in mature microRNAs in high-throughput sequencing libraries. *Genome Res* **20:** 257–264.

The FANTOM Consortium and the Riken Omics Science Center. 2009. The transcriptional network that controls growth arrest and differentiation in a human myeloid leukemia cell line. *Nat Genet* **41:** 553–562.

Forstemann K, Horwich MD, Wee L, Tomari Y, Zamore PD. 2007. *Drosophila* microRNAs are sorted into functionally distinct argonaute complexes after production by dicer-1. *Cell* **130:** 287–297.

Ghildiyal M, Xu J, Seitz H, Weng Z, Zamore PD. 2010. Sorting of *Drosophila* small silencing RNAs partitions microRNA* strands into the RNA interference pathway. *RNA* **16:** 43–56.

Glazov EA, Cottee PA, Barris WC, Moore RJ, Dalrymple BP, Tizard ML. 2008. A microRNA catalog of the developing chicken embryo identified by a deep sequencing approach. *Genome Res* **18:** 957–964.

Griffiths-Jones S, Saini HK, van Dongen S, Enright AJ. 2008. miRBase: Tools for microRNA genomics. *Nucleic Acids Res* **36:** D154–D158.

Grimson A, Srivastava M, Fahey B, Woodcroft BJ, Chiang HR, King N, Degnan BM, Rokhsar DS, Bartel DP. 2008. Early origins and evolution of microRNAs and Piwi-interacting RNAs in animals. *Nature* **455:** 1193–1197.

Hagan JP, Piskounova E, Gregory RI. 2009. Lin28 recruits the TUTase Zcchc11 to inhibit let-7 maturation in mouse embryonic stem cells. *Nat Struct Mol Biol* **16:** 1021–1025.

Han J, Lee Y, Yeom KH, Nam JW, Heo I, Rhee JK, Sohn SY, Cho Y, Zhang BT, Kim VN. 2006. Molecular basis for the recognition of primary microRNAs by the Drosha–DGCR8 complex. *Cell* **125:** 887–901.

Heo I, Joo C, Kim YK, Ha M, Yoon MJ, Cho J, Yeom KH, Han J, Kim VN. 2009. TUT4 in concert with Lin28 suppresses microRNA biogenesis through pre-microRNA uridylation. *Cell* **138:** 696–708.

Hock J, Meister G. 2008. The Argonaute protein family. *Genome Biol* **9:** 210.

Hutvagner G, Simard MJ. 2008. Argonaute proteins: Key players in RNA silencing. *Nat Rev Mol Cell Biol* **9:** 22–32.

Ivanovska I, Ball AS, Diaz RL, Magnus JF, Kibukawa M, Schelter JM, Kobayashi SV, Lim L, Burchard J, Jackson AL, et al. 2008. MicroRNAs in the miR-106b family regulate p21/CDKN1A and promote cell cycle progression. *Mol Cell Biol* **28:** 2167–2174.

Jones MR, Quinton LJ, Blahna MT, Neilson JR, Fu S, Ivanov AR, Wolf DA, Mizgerd JP. 2009. Zcchc11-dependent uridylation of microRNA directs cytokine expression. *Nat Cell Biol* **11:** 1157–1163.

Kai ZS, Pasquinelli AE. 2010. MicroRNA assassins: Factors that regulate the disappearance of miRNAs. *Nat Struct Mol Biol* **17:** 5–10.

Katoh T, Sakaguchi Y, Miyauchi K, Suzuki T, Kashiwabara S, Baba T. 2009. Selective stabilization of mammalian microRNAs by 3′ adenylation mediated by the cytoplasmic poly(A) polymerase GLD-2. *Genes Dev* **23:** 433–438.

Kawamata T, Seitz H, Tomari Y. 2009. Structural determinants of miRNAs for RISC loading and slicer-independent unwinding. *Nat Struct Mol Biol* **16:** 953–960.

Koralov SB, Muljo SA, Galler GR, Krek A, Chakraborty T, Kanellopoulou C, Jensen K, Cobb BS, Merkenschlager M, Rajewsky N, et al. 2008. Dicer ablation affects antibody diversity and cell survival in the B lymphocyte lineage. *Cell* **132:** 860–874.

Kwak JE, Drier E, Barbee SA, Ramaswami M, Yin JC, Wickens M. 2008. GLD2 poly(A) polymerase is required for long-term memory. *Proc Natl Acad Sci* **105:** 14644–14649.

Lal A, Navarro F, Maher CA, Maliszewski LE, Yan N, O'Day E, Chowdhury D, Dykxhoorn DM, Tsai P, Hofmann O, et al. 2009. miR-24 Inhibits cell proliferation by targeting E2F2, MYC, and other cell-cycle genes via binding to "seedless" 3′ UTR microRNA recognition elements. *Mol Cell* **35:** 610–625.

Landgraf P, Rusu M, Sheridan R, Sewer A, Iovino N, Aravin A, Pfeffer S, Rice A, Kamphorst AO, Landthaler M, et al. 2007. A mammalian microRNA expression atlas based on small RNA library sequencing. *Cell* **129:** 1401–1414.

Lassmann T, Hayashizaki Y, Daub CO. 2009. TagDust—a program to eliminate artifacts from next generation sequencing data. *Bioinformatics* **25:** 2839–2840.

le Sage C, Nagel R, Egan DA, Schrier M, Mesman E, Mangiola A, Anile C, Maira G, Mercatelli N, Ciafre SA, et al. 2007. Regulation of the $p27^{Kip1}$ tumor suppressor by miR-221 and miR-222 promotes cancer cell proliferation. *EMBO J* **26:** 3699–3708.

Lehrbach NJ, Armisen J, Lightfoot HL, Murfitt KJ, Bugaut A, Balasubramanian S, Miska EA. 2009. LIN-28 and the poly(U) polymerase PUP-2 regulate let-7 microRNA processing in *Caenorhabditis elegans*. *Nat Struct Mol Biol* **16:** 1016–1020.

Li J, Yang Z, Yu B, Liu J, Chen X. 2005. Methylation protects miRNAs and siRNAs from a 3′-end uridylation activity in *Arabidopsis*. *Curr Biol* **15:** 1501–1507.

Liu J, Carmell MA, Rivas FV, Marsden CG, Thomson JM, Song JJ, Hammond SM, Joshua-Tor L, Hannon GJ. 2004. Argonaute2 is the catalytic engine of mammalian RNAi. *Science* **305:** 1437–1441.

Livak KJ, Schmittgen TD. 2001. Analysis of relative gene expression data using real-time quantitative PCR and the $2^{-\Delta\Delta C(T)}$ method. *Methods* **25:** 402–408.

Lu S, Sun YH, Chiang VL. 2009. Adenylation of plant miRNAs. *Nucleic Acids Res* **37:** 1878–1885.

Luzi E, Marini F, Sala SC, Tognarini I, Galli G, Brandi ML. 2008. Osteogenic differentiation of human adipose tissue-derived stem cells is modulated by the miR-26a targeting of the SMAD1 transcription factor. *J Bone Miner Res* **23:** 287–295.

Marson A, Levine SS, Cole MF, Frampton GM, Brambrink T, Johnstone S, Guenther MG, Johnston WK, Wernig M, Newman J, et al. 2008. Connecting microRNA genes to the core transcriptional regulatory circuitry of embryonic stem cells. *Cell* **134:** 521–533.

Martin G, Keller W. 2007. RNA-specific ribonucleotidyl transferases. *RNA* **13:** 1834–1849.

Matranga C, Tomari Y, Shin C, Bartel DP, Zamore PD. 2005. Passenger-strand cleavage facilitates assembly of siRNA into Ago2-containing RNAi enzyme complexes. *Cell* **123:** 607–620.

Mayr C, Bartel DP. 2009. Widespread shortening of 3′ UTRs by alternative cleavage and polyadenylation activates oncogenes in cancer cells. *Cell* **138:** 673–684.

Mayr C, Hemann MT, Bartel DP. 2007. Disrupting the pairing between let-7 and Hmga2 enhances oncogenic transformation. *Science* **315:** 1576–1579.

Meister G, Landthaler M, Patkaniowska A, Dorsett Y, Teng G, Tuschl T. 2004. Human Argonaute2 mediates RNA cleavage targeted by miRNAs and siRNAs. *Mol Cell* **15:** 185–197.

Mellman DL, Gonzales ML, Song C, Barlow CA, Wang P, Kendziorski C, Anderson RA. 2008. A PtdIns4,5P2-regulated nuclear poly(A) polymerase controls expression of select mRNAs. *Nature* **451:** 1013–1017.

Muljo SA, Kanellopoulou C, Aravind L. 2009. MicroRNA targeting in mammalian genomes: Genes and mechanisms. *Wiley Interdiscip Rev Syst Biol Med* **2:** 148–161.

Nakanishi T, Kubota H, Ishibashi N, Kumagai S, Watanabe H, Yamashita M, Kashiwabara S, Miyado K, Baba T. 2006. Possible role of mouse poly(A) polymerase mGLD-2 during oocyte maturation. *Dev Biol* **289:** 115–126.

Petrocca F, Vecchione A, Croce CM. 2008a. Emerging role of miR-106b-25/miR-17-92 clusters in the control of transforming growth factor beta signaling. *Cancer Res* **68:** 8191–8194.

Petrocca F, Visone R, Onelli MR, Shah MH, Nicoloso MS, de Martino I, Iliopoulos D, Pilozzi E, Liu CG, Negrini M, et al. 2008b. E2F1-regulated microRNAs impair TGFbeta-dependent cell-cycle arrest and apoptosis in gastric cancer. *Cancer Cell* **13:** 272–286.

Ramachandran V, Chen X. 2008. Degradation of microRNAs by a family of exoribonucleases in *Arabidopsis*. *Science* **321:** 1490–1492.

Rand TA, Petersen S, Du F, Wang X. 2005. Argonaute2 cleaves the anti-guide strand of siRNA during RISC activation. *Cell* **123:** 621–629.

Scott GK, Mattie MD, Berger CE, Benz SC, Benz CC. 2006. Rapid alteration of microRNA levels by histone deacetylase inhibition. *Cancer Res* **66:** 1277–1281.

Severin J, Waterhouse AM, Kawaji H, Lassmann T, van Nimwegen E, Balwierz PJ, de Hoon ML, Hume DA, Carninci P, Hayashizaki Y, et al. 2009. FANTOM4 EdgeExpressDB: an integrated database of promoters, genes, microRNAs, expression dynamics and regulatory interactions. *Genome Biol* **10:** r39. doi: 10.1186/gb-2009-10-4-r39.

Suh N, Jedamzik B, Eckmann CR, Wickens M, Kimble J. 2006. The GLD-2 poly(A) polymerase activates gld-1 mRNA in the *Caenorhabditis elegans* germ line. *Proc Natl Acad Sci* **103:** 15108–15112.

Taft RJ, Glazov EA, Cloonan N, Simons C, Stephen S, Faulkner GJ, Lassmann T, Forrest AR, Grimmond SM, Schroder K, et al. 2009. Tiny RNAs associated with transcription start sites in animals. *Nat Genet* **41:** 572–578.

Tomari Y, Du T, Zamore PD. 2007. Sorting of *Drosophila* small silencing RNAs. *Cell* **130:** 299–308.

Tomaru Y, Nakanishi M, Miura H, Kimura Y, Ohkawa H, Ohta Y, Hayashizaki Y, Suzuki M. 2009. Identification of an inter-transcription factor regulatory network in human hepatoma cells by Matrix RNAi. *Nucleic Acids Res* **37:** 1049–1060.

Trippe R, Sandrock B, Benecke BJ. 1998. A highly specific terminal uridylyl transferase modifies the 3′-end of U6 small nuclear RNA. *Nucleic Acids Res* **26:** 3119–3126.

Ventura A, Young AG, Winslow MM, Lintault L, Meissner A, Erkeland SJ, Newman J, Bronson RT, Crowley D, Stone JR, et al. 2008. Targeted deletion reveals essential and overlapping functions of the miR-17 through 92 family of miRNA clusters. *Cell* **132:** 875–886.

Wang L, Eckmann CR, Kadyk LC, Wickens M, Kimble J. 2002. A regulatory cytoplasmic poly(A) polymerase in *Caenorhabditis elegans*. *Nature* **419:** 312–316.

Xiao C, Srinivasan L, Calado DP, Patterson HC, Zhang B, Wang J, Henderson JM, Kutok JL, Rajewsky K. 2008. Lymphoproliferative disease and autoimmunity in mice with increased miR-17-92 expression in lymphocytes. *Nat Immunol* **9:** 405–414.

Yoda M, Kawamata T, Paroo Z, Ye X, Iwasaki S, Liu Q, Tomari Y. 2010. ATP-dependent human RISC assembly pathways. *Nat Struct Mol Biol* **17:** 17–23.

Received February 3, 2010; accepted in revised form July 12, 2010.